Inverse response of ^{231}Pa/^{230}Th to variations of the Atlantic Meridional Overturning Circulation in the North Atlantic intermediate water

Finn Süfke[1]*, Hartmut Schulz[2], Jeemijn Scheen[3,4], Sönke Szidat[4,5], Marcel Regelous[6], Patrick Blaser[1], Frerk Pöppelmeier[1], Tyler J. Goepfert[7,8], Thomas F. Stocker[3,4] and Jörg Lippold[1]

[1]Heidelberg University, Institute of Earth Sciences, Heidelberg, Germany
[2]University of Tübingen, Institute of Earth Sciences, Tübingen, Germany
[3]University of Bern, Climate and Environmental Physics, Physics Institute, Bern, Switzerland
[4]University of Bern, Oeschger Centre for Climate Change Research, Bern, Switzerland
[5]University of Bern, Department of Chemistry and Biochemistry, Bern, Switzerland
[6]FAU Erlangen-Nürnberg, GeoZentrum Nordbayern, Erlangen, Germany
[7]GEOMAR Helmholtz-Center for Ocean Research Kiel, Kiel, Germany
[8]Arizona State University, School of Earth and Space Exploration, Tempe, AZ, USA

*corresponding author: finn.suefke@geow.uni-heidelberg.de / Tel.: +496221546063
ORCID: 0000 0001 5271 1099

<u>Abstract</u>

This study aims to provide a more detailed understanding of the behavior of ^{231}Pa/^{230}Th under varying ocean circulation regimes. The North Atlantic provides a unique sedimentary setting with its Ice-Rafted-Detritus (IRD) layers deposited during glacial times. These layers have been found north of 40°N (Ruddiman Belt) and are most pronounced during Heinrich Stadials. Most of these sediments have been recovered from the deep North Atlantic basin typically below 3000 m water depth. This study reports sedimentological and sediment geochemical data from one of the few sites at intermediate depth of the open North Atlantic (core SU90-I02, 45°N 39°W, 1965 m water depth) within the Ruddiman Belt. The time periods of Heinrich Stadials 1 and 2 of this core were identified with the help of the major element composition by XRF scanning and by IRD counting. Along the core profile the sedimentary ^{231}Pa/^{230}Th activity ratio has been measured as a kinematic proxy for the circulation strength. The ^{231}Pa/^{230}Th record shows highest values during the Holocene and LGM, above the natural production ratio of these isotopes. During Heinrich Stadial 1 and 2, when AMOC was most reduced, the ^{231}Pa/^{230}Th record shows overall lowest values below the production ratio. This behavior is contrary to classical findings of ^{231}Pa/^{230}Th from the northwestern Atlantic where a strong Holocene circulation is associated with low values. However, this behavior at the presented location is in agreement with results from simulations of the ^{231}Pa/^{230}Th-enabled Bern3D Earth System Model.

source: https://doi.org/10.7892/boris.141787 | downloaded: 4.5.2023

1. Introduction

Changes in the paleoclimate of the North Atlantic region have been related to variations in the Atlantic Meridional Overturning Circulation (AMOC) on glacial-interglacial down to millennial scale timescales as observed from deep marine sediments (e.g. Lynch-Stieglitz, 2017). One example of the sedimentary features of the North Atlantic is the episodic occurrence of distinguished layers of terrigenous sediments ranging from detrital carbonate to cm-wide clastic rocks in sediments north of 40°N (Ruddiman Belt; Ruddiman, 1977). These prominent sediment layers are associated with discharge-events of icebergs originated from the Labrador Sea and are known as Ice Rafted Detritus (IRD) or Heinrich layers (Heinrich, 1988; Andrews and Tedesco, 1992; Bond et al., 1992; Broecker et al., 1992; Hemming, 2004). Heinrich layers have been the target of a great amount of studies aiming for understanding their origin, climatic background and consequence (Heinrich, 1988; Andrews and Tedesco, 1992; Bond et al., 1992; Broecker et al., 1992; Grousset et al., 2001; Hemming, 2004, Rashid and Boyle, 2007; Hodell et al., 2008; Bradtmiller et al., 2014; Hodell et al., 2017, Andrews and Voelker, 2018). Most paleoclimatologic studies agree that Heinrich layers are associated with Heinrich Stadials, climate periods on millennial scales with an extraordinary cold and dry climate. Large inputs of freshwater into the North Atlantic are a common feature of Heinrich Stadials (e.g. Duplessy et al., 1992; Clark et al., 2001; Roche et al., 2004). Since the North Atlantic region and its adjacent seas are key regions for the AMOC with their deep water formation zones, the AMOC is highly sensitive to abrupt changes by e.g. freshwater input into the area (McManus et al., 2004). One consequence is the reorganization of water mass distributions in the Atlantic during Heinrich Stadials (e.g. Henry et al., 2016).

The reconstruction of changes in AMOC strength is often enabled with the kinematic circulation strength proxy $^{231}Pa/^{230}Th_{(xs,0)}$. The radioisotopes ^{231}Pa and ^{230}Th are the radioactive decay products of ^{235}U and ^{234}U, respectively. Uranium is homogenously dissolved in the world ocean and decays to ^{231}Pa and ^{230}Th at a constant activity ratio of 0.093 (so called "production ratio"; Henderson and Anderson, 2003). In contrast to uranium, protactinium and thorium are highly particle-reactive elements with residence times in the range of ~150 and ~20 years, respectively (Henderson and Anderson, 2003). The higher residence time of protactinium is caused by its lower affinity to particles in the water column, compared to thorium. The resulting fractionation, due to particle reactivity, is the key process of the $^{231}Pa/^{230}Th$ proxy. While ^{230}Th is virtually scavenged completely from the water column after production, ^{231}Pa can be laterally advected by deep water currents on a basin scale. Therefore, high ratios indicate slow circulation and vice versa. Accordingly, $^{231}Pa/^{230}Th$ is anti-correlated with the basin-scale circulation strength (e.g. Yu et al., 1996; McManus et al., 2004). However, protactinium shows a high affinity to biogenic opal (Chase et al., 2003), which acts as an effective sink for protactinium (e.g. in the Southern Ocean; Rutgers van der Loeff et al., 2016) potentially obscuring its circulation signal.

Furthermore, the usage of the $^{231}Pa/^{230}Th$ proxy is complicated in regions of high particle fluxes and weak deep water advection such as ocean margins (Anderson et al., 1983; Hayes et al., 2015a). In contrast, the role of Ice Rafted Detritus (IRD) and lithogenic particles in general is thought to be of minor importance on the scavenging behavior of ^{231}Pa (Chase et al., 2002,2004; Roberts et al., 2014).

The expected anti-correlated response of $^{231}Pa/^{230}Th$ to AMOC strength has been demonstrated by several model approaches (Gu and Liu, 2017; Marchal et al., 2000; Siddall et al., 2007; Rempfer et al., 2017), and represents a general feature in the deep West Atlantic (McManus et al., 2004; Gherardi et al., 2005; Bradtmiller et al., 2007; Gherardi et al., 2009; Lippold et al., 2012a; Bradtmiller et al., 2014; Böhm et al., 2015; Henry et al., 2016; Lippold et al., 2016; Mulitza et al., 2017; Voigt et al., 2017; Ng et al., 2018; Waelbroeck et al., 2018; Süfke et al., 2019). However, a number of downcore profiles from the shallower North Atlantic give a different picture of high $^{231}Pa/^{230}Th$ during the Holocene despite its evident strong export of North Atlantic Deep Water (NADW) (Hall et al., 2006; Gherardi et al., 2009; Lippold et al., 2012a, 2012b, 2016) and therefore the generally accepted notion of a pronounced ^{231}Pa export (Deng et al., 2018). This contradictory behavior, however, has been already predicted for the shallower northern North Atlantic by models of simple and intermediate complexity (Luo et al., 2010; Rempfer et al., 2017). In particular, Rempfer et al. (2017) noted that the area north of ~40°N and above 2500 m water depth is supposed to show a positive correlation between $^{231}Pa/^{230}Th$ and AMOC strength based on the Bern3D model.

This study aims to provide a deeper understanding of the relation between $^{231}Pa/^{230}Th$ and AMOC strength variations by presenting a new $^{231}Pa/^{230}Th$ downcore profile from the mid-depth North Atlantic at 45°N. The $^{231}Pa/^{230}Th$ profile is complemented by foraminifera abundance data and the information of the sedimentary composition by XRF scanning, IRD counting and biogenic opal content that were analyzed to identify and investigate the impact of climate events like Heinrich Stadial 1 and 2 on the research area.

2. Methods and Material

2.1. Core location and age model

In this study sediments from interface core SU90-I02 with a total length of 43 cm on top of one of the easternmost Milne Seamounts (45°05’ N, 39°26’ W) at 1965 m water depth were analyzed (Fig. 1). The Milne Seamounts are located in the open North Atlantic east from the Grand Banks of Newfoundland. The investigated site lies within the Ruddiman Belt (Ruddiman, 1977) and sediments deposited before the Holocene are therefore characterized by high amounts of IRD. Today the core site is bathed by Labrador Sea Water which is part of southward flowing NADW (Ferreira and Kerr, 2017).

The general core chronology is based on the correlation of the δ^{18}O record to other records of the North Atlantic region (Fig. S2) and was refined by four ^{14}C Accelerator Mass Spectrometry (AMS) dates. The new radiocarbon-based age tie-point dates have been measured at the LARA laboratory at the University of Bern, Switzerland (Szidat et al., 2014; Gottschalk et al., 2018). The CALIB 7.1 online tool tied to the Marine13 calibration curve was used (Reimer et al., 2013) with a 400 year reservoir age correction (Table S1).

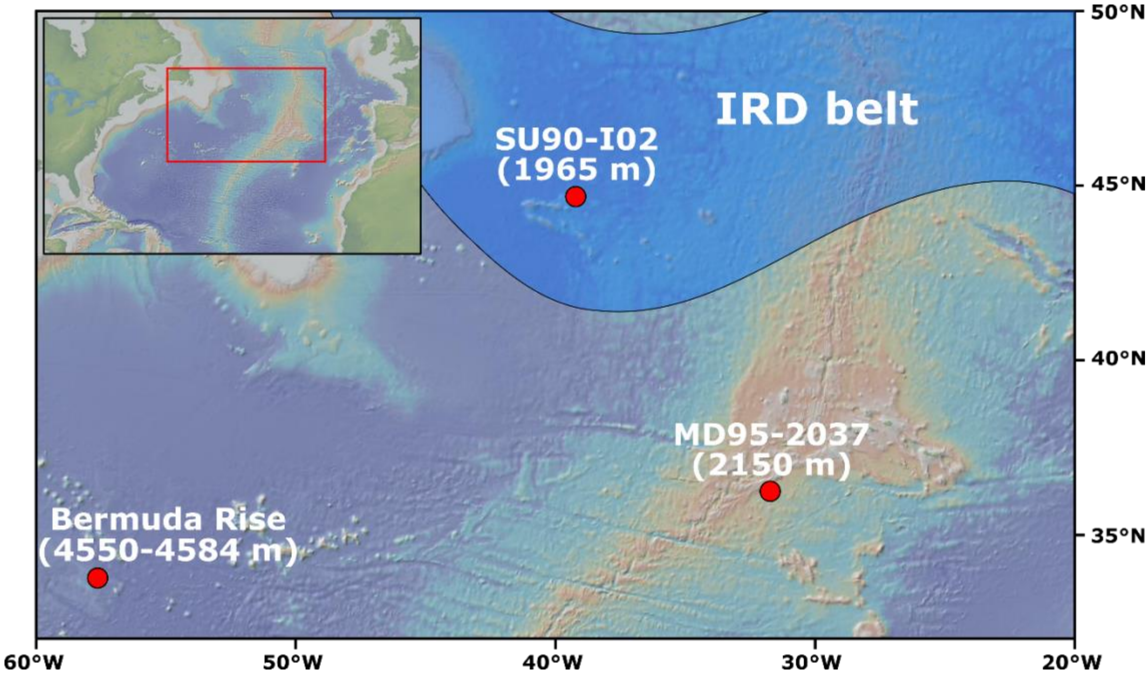

Fig. 1 Overview map of the northern North Atlantic region with the position of core SU90-I02 (45°05'N 39°26'W) on the Milne Seamounts, MD95-2037 (37°05'N 32°01'W; Gherardi et al., 2009) and the Bermuda Rise site (OCE329-GGC5: 33°42'N 57°35'W, McManus et al., 2004; ODP 1063: 33°41'N 57°37'W, Lippold et al., 2009). Number in brackets indicate the water depth of the sites. The blue shaded area depicts the main area of IRD depositions during Heinrich Events 1 and 2 (after Hemming, 2004).

2.2. Analytical methods

The light-colored sandy sediments of interface core SU90-I02 were first sampled continuously in July 1990 on board of the research vessel Le Suroit at 2 cm intervals down to 42.5 cm core depth. These samples were used for investigation of the foraminifera assemblage, stable isotope analyses, radiocarbon dating and IRD counting on the washed sand fraction. Later in 2018, the last available series of bulk sediment samples was collected from Bordeaux University (EPOC) for sedimentary ^{231}Pa/^{230}Th, XRF and opal analysis (Table S1). This sample series covers continuously the whole core but with discontinuous sample widths up to 2.5 cm (Table S1). Sample splits from the first sample series for planktic foraminifera analyses were freeze-dried, wet-sieved over a 63 µm screen, and oven-dried at 40°C. Counts were conducted on the whole residue or on splits of the size fraction >150 µm and examined under a stereo-dissecting microscope in order to obtain the sand fraction of >150 µm and to quantify the inorganic (IRD counts) and microfossil (foraminifera) components. Planktic foraminifera were identified to the species level (Banner and Blow, 1960; Bandy, 1972; Kucera, 2007; Storz et al., 2009; Schiebel and Hemleben, 2017). Foraminifera samples of *Neogloboquadrina pachyderma sinistral* were cracked and cleaned with methanol in an ultra-sonic bath before $\delta^{18}O$ analysis. The $\delta^{18}O$ analysis (Schulz, 1995b) were carried out in the former Institute for Pure and Applied Nuclear Physics at the University of Kiel, Germany.

Separation and purification of protactinium, uranium and thorium isotopes from sediment samples of SU90-I02 followed the protocol described by Süfke et al. (2018). Samples were spiked with ^{229}Th, ^{236}U and ^{233}Pa before total dissolution in a mixture of concentrated HCl, HNO_3 and HF, which was then followed by further chemical purification by column chromatography. Since ^{233}Pa is a short lived isotope ($t_{1/2}$= 27 d) it had been milked from a ^{237}Np solution (Regelous et al., 2004) directly before the chemical treatment and purification of the samples. The ^{233}Pa spike was calibrated against the reference materials UREM-11 (Süfke et al., 2018), IAEA-385 (Pham et al., 2008) and an internal pitchblende standard (Fietzke et al., 1999). Finally, concentrations of the radioisotopes ^{230}Th, ^{231}Pa, ^{232}Th, ^{234}U, and ^{238}U were measured with a Neptune Plus MC-ICP-MS at the Geozentrum Nordbayern in Erlangen, Germany.

For the calculation of $^{231}Pa_{excess}$ and $^{230}Th_{excess}$ from measured bulk ^{231}Pa and ^{230}Th a detrital correction of $^{238}U/^{232}Th$ = 0.55 has been applied (Henderson and Anderson, 2003). This correction is in agreement with the overall minimum of bulk $^{238}U/^{232}Th$ in the samples of SU90-I02 and within typical lithogenic activity ratios (0.5 to 0.6) found in the western Atlantic sector (Henderson and Anderson, 2003). Variations in the detrital correction do not show a significant effect on the age corrected sedimentary $^{231}Pa/^{230}Th_{excess}$ record (Lippold et al., 2016; Missiaen et al., 2018; Fig. S1) even for time periods of distinctly different sedimentation regimes (e.g. Heinrich Events). This argues in favor of a negligible impact of the lithogenic particle flux on the resulting $^{231}Pa/^{230}Th_{excess}$ record. ^{231}Pa and ^{230}Th excess concentrations were decay corrected to the time of deposition. All individual isotope concentrations are provided in the supplement (Table S1).

To investigate the potential influence of biogenic opal on ^{231}Pa (Chase et al., 2002, 2003; Rutgers van der Loeff et al., 2016) the sedimentary opal concentration was analyzed by automated leaching following the procedure described by Müller and Schneider (1993). Furthermore, the major element composition (Al, Si, K, Ca, Ti and Sr) of discrete bulk sediment samples were analyzed with a fourth generation Avaatech XRF core scanner at the Institute of Earth Sciences at Heidelberg University, Germany. Elemental ratios (e.g. Ca/Sr) are a useful tool to identify Heinrich-Layers in the North Atlantic (Hodell et al., 2008).

3. Results

<u>3.1. Age model refinement by ^{14}C and $\delta^{18}O$</u>

The core chronology was established for SU90-I02 based on stable oxygen isotope data (Schulz, 1995b), as well as on four ^{14}C dates. The radiocarbon dates at sediment depths of 21 and 33 cm were obtained from *N. pachyderma s.* and give absolute ages of 9 and 22.5 ka BP, respectively. Radiocarbon dates from sediment depths 9 and 19 cm were obtained from *Globigerina bulloides* and give absolute ages of 6.3 and 7.3 ka BP, respectively (Fig. 2; Table S1). A potential negative influence of analyzing different species for radiocarbon dating on the accuracy of the age model is possible but has been found not to be significant for the here investigated species and time periods (Manighetti et al., 1995). For a further refinement of the age model the planktonic $\delta^{18}O$ record of *N. pachyderma s*. (Schulz, 1995b) was correlated to established $\delta^{18}O$ records from the North Atlantic IRD belt (Bond et al., 1992; Labeyrie et al., 1995; Grousset et al., 2001; Jullien et al., 2006; Rashid and Boyle, 2007; Hodell et al., 2017; Fig. S2). All records from the before mentioned studies show a consistent picture of a shift in planktic $\delta^{18}O$ (from *N. pachyderma s.*) to lighter values between 17 and 17.5 ka right before the major IRD depositions of Heinrich Stadial 1, as seen at 24 cm core depth in SU90-I02 (Fig. 2). Further, the slight shift from lighter to heavier $\delta^{18}O$ at 35 cm in SU90-I02 can be correlated to a similar shift in $\delta^{18}O$ observed in the North Atlantic during Heinrich Stadial 2 between 24 and 25 ka (Broecker et al., 1990/1992; Jullien et al., 2006; Rashid and Boyle, 2007). The increase in $\delta^{18}O$ in the deeper part of the presented record can be related to a warm phase between Heinrich Stadial 2 and 3 (Heinrich 1988; Broecker et al., 1990; Bond et al., 1992).

With these age constraints a hiatus in SU90-I02 is apparent in the depth below 21 cm (Fig. S3). While the onset of Heinrich Layer 1 is present at 24 cm (see section 4.1.) the late Heinrich Stadial 1, the Younger Dryas, the Bølling/Allerød and the very early Holocene parts are missing (Fig. S3). Additionally, it has to be kept in mind that the exact timing and duration of SU90-I02 variations in $^{231}Pa/^{230}Th$ and XRF samples are less well defined since these samples integrate up to 2.5 cm of sediment (Table S1). Sample widths of 2.5 cm can integrate up to 1000 years in SU90-I02 and therefore limit the time resolution.

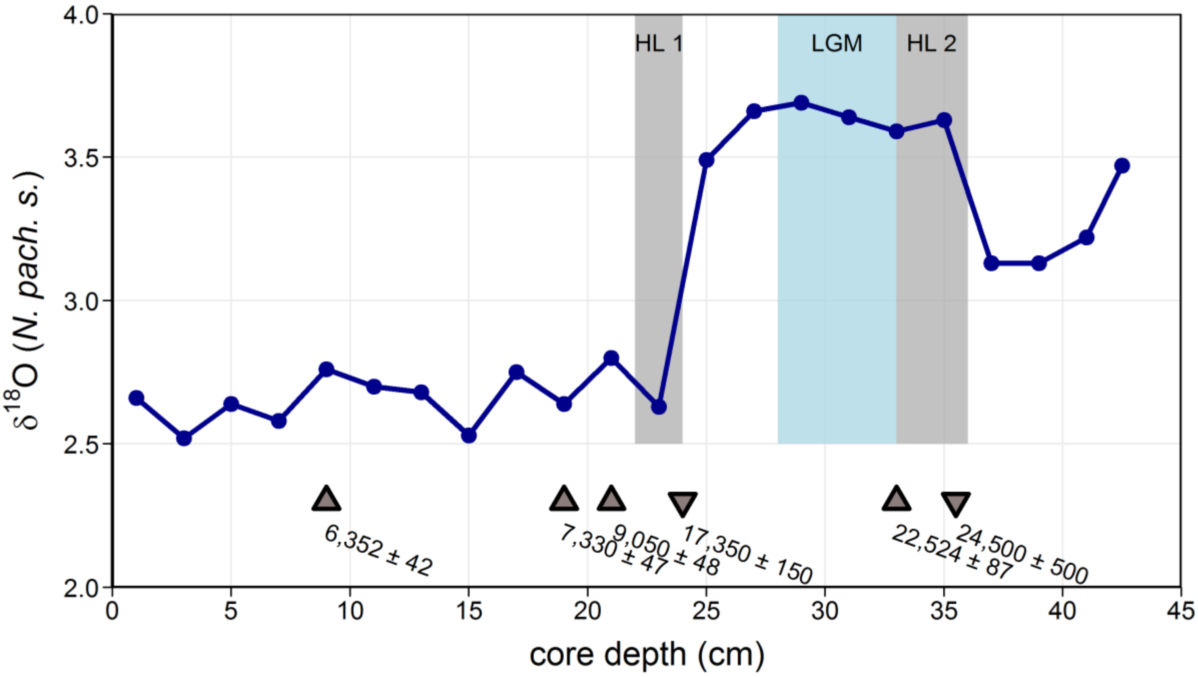

Fig. 2 The $\delta^{18}O$ record of the planktic foraminifera *N. pachyderma s* (Schulz, 1995b). Upward triangles indicate ^{14}C dates and downward triangle age tie points derived from $\delta^{18}O$ (cf. section 3.1.). Gray bars show the position of Heinrich Layers 1 (HL 1) and 2 (HL 2) (based on IRD and foraminifera data; see Fig. 3, 4) and the blue bar indicate the Last Glacial Maximum (LGM) section of SU90-I02.

3.2. Radioisotope analysis

The $^{231}Pa/^{230}Th$ profile for SU90-I02 displays high values between 0.083 and 0.116 in the upper 15 cm of the core corresponding to the Holocene period (Fig. 3a). Further, at 29 cm core depth a sharp peak in $^{231}Pa/^{230}Th$ reaches 0.130, which is the highest value of the entire record, and is related to the LGM. Between 17 and 24 cm and below 33 cm $^{231}Pa/^{230}Th$ values are quite stable between 0.06 and 0.07. These intervals are related to the early Holocene as well as Heinrich Stadials 1 and 2, respectively.

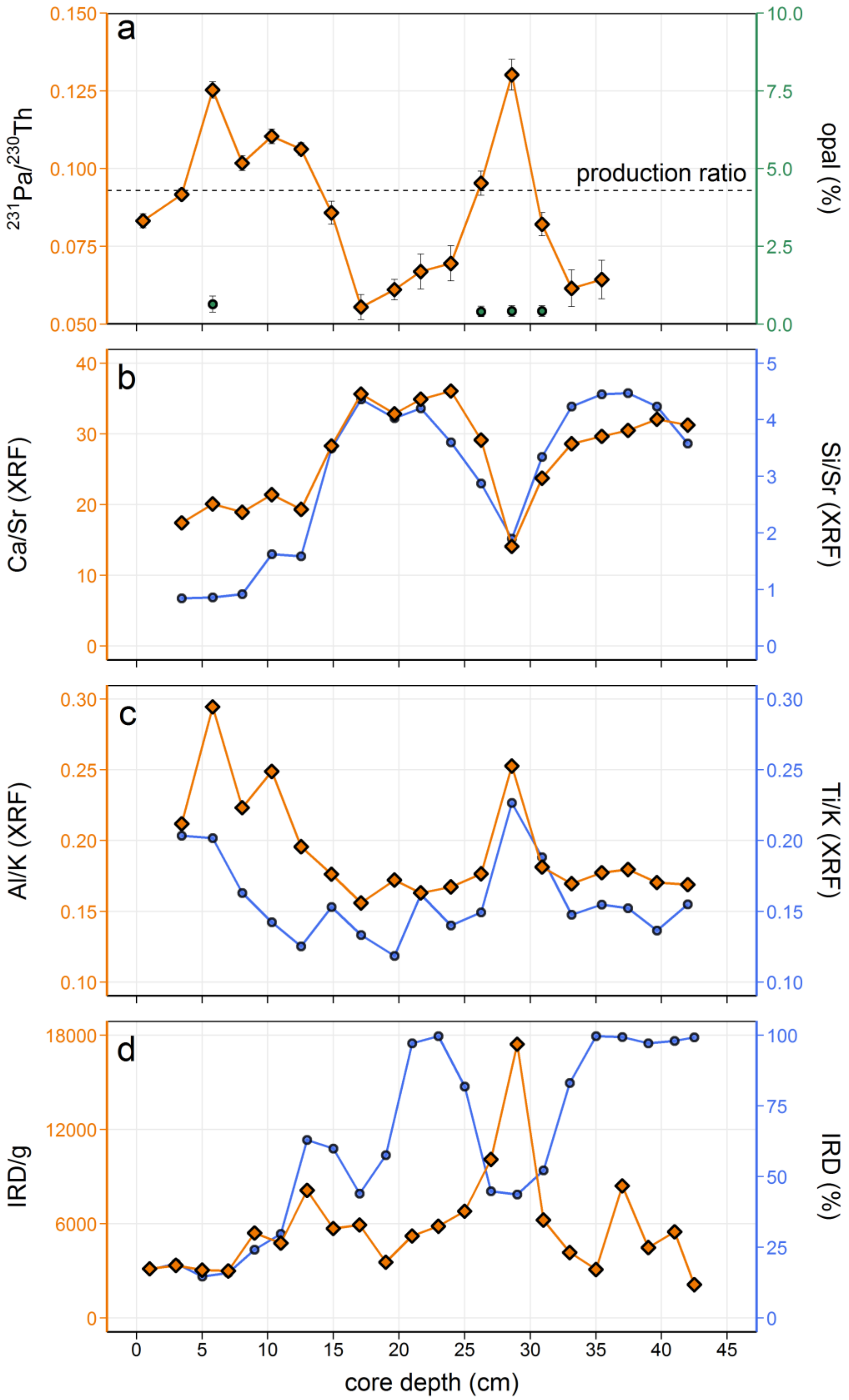

Fig. 3 Geochemical and sedimentary parameters of SU90-I02. (a) $^{231}Pa/^{230}Th$ activity ratios and opal concentration (%). The dashed line indicates the production ratio of $^{231}Pa/^{230}Th$. (b, c) Bulk element ratios of Ca/Sr, Si/Sr, Al/K and Ti/K measured on discrete sediment samples by XRF. (d) Absolute IRD counts of the bulk sediment and relative IRD percentages in the >150 μm fraction.

3.3. Sedimentary analysis of foraminifera, opal and major elements

Planktic foraminifera of the species *Neogloboquadrina pachyderma sinistral, Neogloboquadrina pachyderma dextral (also called Neogloboquadrina incompta; Schiebel and Hemleben, 2017)* and *Globigerina bulloides* were investigated for this study (Fig. 4a/b/c) as representatives for a colder/glacial (*N. pachyderma s.)* and more moderate (*N. pachyderma d*. and *G. bulloides*) environment (e.g. Manighetti et al., 1995). Species *N. pachyderma d*. and *G. bulloides* show their highest abundances in the top 10 cm of the core. Below 10 cm, *N. pachyderma s.* is the dominant species throughout the record. In the interval between 19 and 25 cm core depth (including Heinrich Stadial 1) all species show an abundance minimum (e.g. *Heinrich, 1988*). The following interval between 25 and 33 cm (LGM) is characterized by the reappearance of all species. While *N. pachyderma d*. and *G. bulloides* reached Holocene levels at 29 cm, *N. pachyderma s.* is the most dominant species with a relative abundance of 75 % of all foraminifera (Fig. 4a). Below 33 cm all species vanish again to extremely low abundance rates (Heinrich Stadial 2).

The sedimentary composition is monitored by major element analysis as well as opal concentration measurements and IRD counts (Fig 3; Table S1). Opal concentrations are constantly very low (< 1 %) throughout the presented record (Fig. 3a). In contrast, major element ratios show a distinct pattern. Ca/Sr and Si/Sr ratios are low in the top 17 cm of the core. Between 17 and 26 cm (including Heinrich Stadial 1) highest values of these ratios are found. At 29 cm (LGM) both ratios return to low values as seen during the Holocene. Below 29 cm ratios for Ca/Sr and Si/Sr return again to higher values like seen during Heinrich Stadial 1. The lithogenic element ratios Al/K and Ti/K show high values in the top 7 cm, which then decrease to the overall lowest ratios in the interval downcore to 26 cm. At 29 cm both lithogenic element ratios return to Holocene-like values but sharply decrease back to low ratios below. The course of the XRF measurements is mirrored by the IRD counts (Fig. 3d). During intervals of high Ca/Sr ratios (21 to 25 and 35 to 42 cm) the percentage of IRD in the >150 µm fraction is nearly 100 %. Lowest IRD percentages are visible in the top 10 cm of the core (Holocene) and around 29 cm (LGM). The timing of these periods matches the most pronounced changes in the XRF data, abundances of investigated foraminifera species and $^{231}Pa/^{230}Th$.

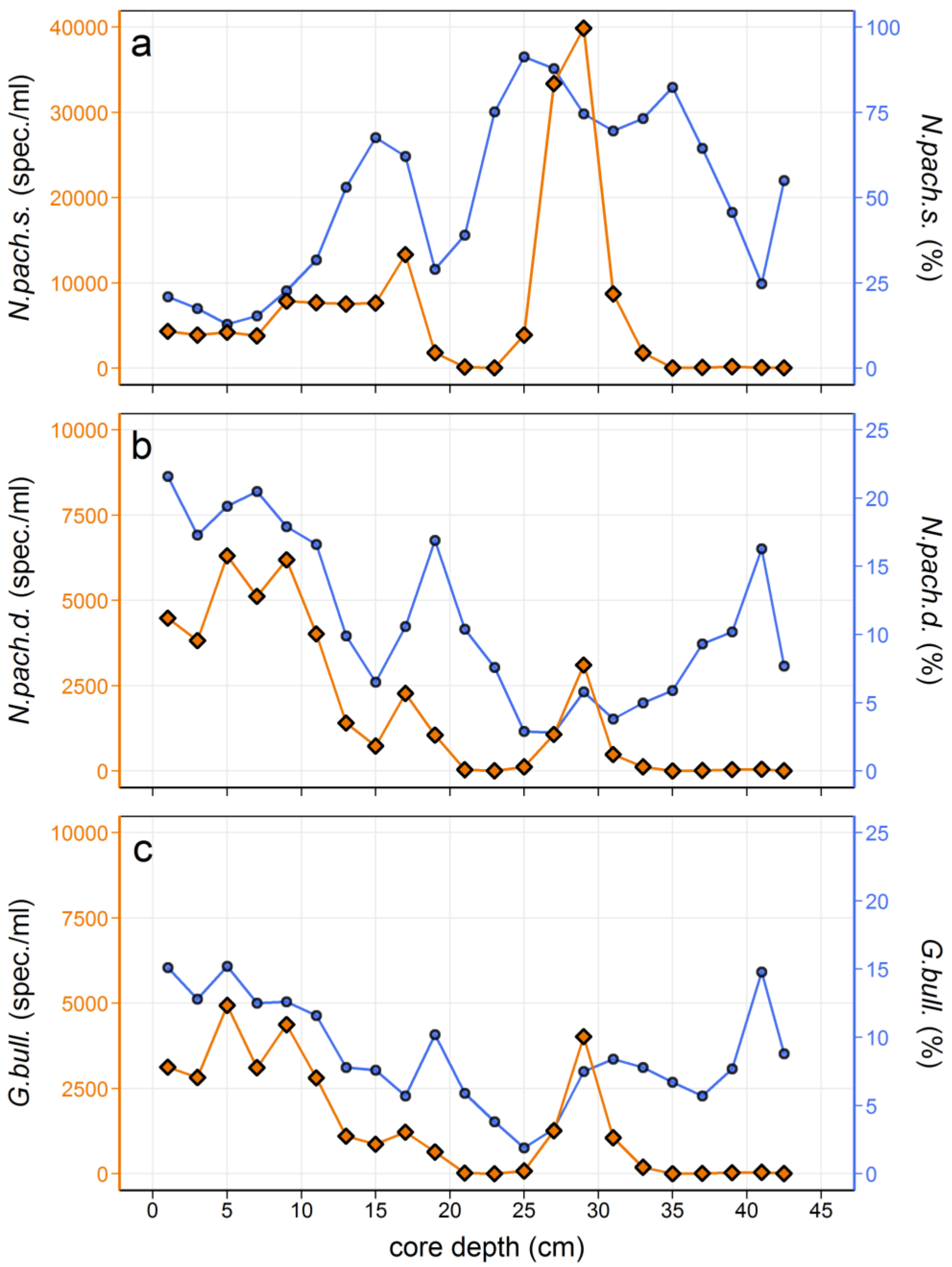

Fig. 4 Absolute (orange; in specimens per ml) and relative (blue; in % of all foraminifera; Schulz, 1995b) abundances of the foraminifera species *N. pachyderma s.* (a), *N. pachyderma d.* (b), and *G. bulloides* (c). Please note the different y-scale for panel a compared to panels b and c.

4. Discussion

4.1. Characterization of Heinrich layers

The core chronology is extended by the identification of Heinrich layers in SU90-I02. Heinrich layers are characterized by detrital carbonate which can easily be identified in North Atlantic sediments by its high Ca/Sr signature compared to regular marine sediments (Hodell et al., 2008). In SU90-I02 highest Ca/Sr ratios were identified in the depth interval between 15 and 25 cm as well as below 30 cm down to 42 cm (Fig. 3b). The course of Ca/Sr is also reflected in Si/Sr, which indicates the presence of silicate-rich IRDs (Hodell et al., 2008; Fig. 3b). Accompanied by the relative amount of IRD in the >150 µm fraction (IRD %; Fig. 3d), with highest values of nearly 100 % of IRD between 21 and 25 cm as well as below 33 cm, both these intervals can be assigned to Heinrich Layers 1 and 2, respectively. Both Heinrich layers are interrupted by a sharp decrease in Ca/Sr and Si/Sr at 29 cm (LGM) which occurs at the same interval as absolute foraminifera abundance as well as the ^{231}Pa/^{230}Th record are increased. The low Ca/Sr can be interpreted as absent detrital carbonate and a sediment source different from Heinrich-IRDs inferred from low Si/Sr (Hodell et al., 2008; Hodell et al., 2017). Further, the ratios of the terrigenous elements (Ti/K and Al/K) show an anomaly at the same core depth (Fig. 3c). IRD deposits during Heinrich Events can be linked to a North Canadian source (e.g. Andrews and Tedesco, 1992), while IRDs during the LGM most likely originated from Greenland (Watkins et al., 2007). Additionally, absolute IRD counts are highest at the core depth of 29 cm, while the relative amount of IRD in the >150 µm fraction is much lower (~44 %) than in Heinrich layers. The lower concentrations of IRD during the LGM is the effect of the high abundances of preserved foraminifera diluting the IRD in the >150 µm fraction. In contrast, during Heinrich Stadial 1 and 2 foraminifera are nearly absent in the >150 µm fraction (Fig. 4) caused either by an environment not favorable for foraminifera growth or a massive dilution of foraminifera shells in the sediment by IRDs.

4.2. The role of particle flux on ^{231}Pa/^{230}Th at SU90-I02

The new ^{231}Pa/^{230}Th downcore profile of SU90-I02 displays high Holocene values, above production ratio, preceded by lower values during the intervals of the Heinrich Stadial 1 and 2 interrupted by a distinctive peak of high ^{231}Pa/^{230}Th during the LGM (Fig. 3a). The high sedimentary ^{231}Pa/^{230}Th above the production ratio from a North Atlantic sediment core during the Holocene calls at first glance for a strong influence of particle flux and/or particle composition on protactinium-scavenging (Anderson et al., 1983; Christl et al., 2010). However, preserved opal concentrations, known as an effective scavenger of protactinium (Chase et al., 2003; Rutgers van der Loeff et al., 2016), are low during the Holocene and LGM (Fig. 3a) and thus clearly below the range (>5-10 %) for which any empirical correlation between opal and increased ^{231}Pa/^{230}Th values can be observed in the Atlantic (Lippold et al., 2012a; Ng et al., 2018).

Further, the ^{230}Th normalized sediment flux is lowest when ^{231}Pa/^{230}Th is highest and vice-versa (Fig. 5) arguing against a major influence of particle flux on the temporal evolution of the ^{231}Pa/^{230}Th record. This observation is further corroborated by the ^{230}Th normalized vertical sediment-accumulation rate of around 3 to 7 g/cm^2/ka for the time periods of highest ^{231}Pa/^{230}Th. Similar vertical fluxes have been reported from sites of circulation dominated ^{231}Pa/^{230}Th records (McManus et al., 2004; Gherardi et al., 2009; Roberts et al., 2014). Roberts et al. (2014) also conclude that fluxes of ~5 g/cm^2/ka are not capable of significantly increasing the ^{231}Pa/^{230}Th ratio in a circulation controlled setting. Interestingly, when the ^{230}Th normalized sediment flux is greatest, reaching values up to 20 g/cm^2/ka, ^{231}Pa/^{230}Th is lowest with values clearly below the production ratio. The section featuring the overall highest ^{231}Pa/^{230}Th corresponds to the LGM (around 29 cm) and is characterized by a massive change in sedimentary composition as well as in the environmental boundary conditions. Due to the high abundances of preserved foraminifera and high IRD counts, a certain particle effect on the ^{231}Pa scavenging behavior cannot be excluded but is considered to be of subordinate relevance since these particle types are not of primary importance for the scavenging of protactinium (Chase et al. 2004).

4.3. The effect of sediment winnowing on ^{231}Pa/^{230}Th

For large parts of the ^{231}Pa/^{230}Th profile the sediment core experienced enhanced sediment winnowing (Fig. 5c). Hence, besides the particle type also effects of sediment sorting and selective removal of different sediment phases and grain sizes may have influenced the measured sedimentary ^{231}Pa/^{230}Th ratio (Geibert and Usbeck, 2004; Kretschmer et al., 2010; Kretschmer et al., 2011). Kretschmer et al. (2011) investigated the effect of winnowing (removal) of the fine fraction (< 20 µm) with and without opal-rich particles on the retained sedimentary ^{231}Pa/^{230}Th ratio, since protactinium is characterized by a high affinity to particles built up from biogenic opal while thorium is preferentially scavenged by fine sized particles like clay (e.g. Chase et al., 2002; Geibert and Usbeck, 2004; Rutgers van der Loeff et al., 2016). From opal-rich sediments in the Southern Ocean Kretschmer et al. (2011) found that the removal of the fine fraction (< 20 µm) alone would result in a slightly increased sedimentary ^{231}Pa/^{230}Th ratio since the lost fine particles like clay are a major carrier phase of scavenged ^{230}Th. In contrast, if opal-rich particles, the main carrier phase of scavenged ^{231}Pa, is lost by winnowing the retained ^{231}Pa/^{230}Th ratio can clearly decrease (Kretschmer et al., 2011 and their Fig. 4). Indeed, SU90-I02 shows sediment winnowing prior the Holocene (Fig. 5c) a period which exhibited low ^{231}Pa/^{230}Th markedly below the production ratio. However, since the sedimentary setting of SU90-I02 with its very low opal concentrations (Fig. 3) is very different to the Southern Ocean, winnowing would rather have removed ^{230}Th rich clay particles which should be evident in high ^{231}Pa/^{230}Th. This is not observed here with exception of a short excursion during the LGM. While this excursion could be explained by the removal of clay particles it contradicts the observation of generally low ^{231}Pa/^{230}Th during strong winnowing. Correlations between winnowing and ^{231}Pa/^{230}Th are thus considered too ambiguous for explaining the observed variations in ^{231}Pa/^{230}Th. Furthermore, the effect of sediment sorting on ^{231}Pa/^{230}Th has not been observed yet for winnowing sites and is inferred from findings of Southern Ocean sediments (Kretschmer et al., 2011).

From the observations as outlined in paragraph 4.2. and 4.3. it is concluded that the main features of the $^{231}Pa/^{230}Th$ record of SU90-I02 and the huge variations in absolute $^{231}Pa/^{230}Th$ values cannot have been primarily controlled by variations in particle fluxes, particle compositions or winnowing, but are best explained by large-scale AMOC variations imprinted in the sedimentary $^{231}Pa/^{230}Th$. The uncorrelated or even anti-correlated evolution of $^{231}Pa/^{230}Th$ with sediment fluxes in turn points towards variations in both $^{231}Pa/^{230}Th$ and sedimentation history along with changes in the circulation regime.

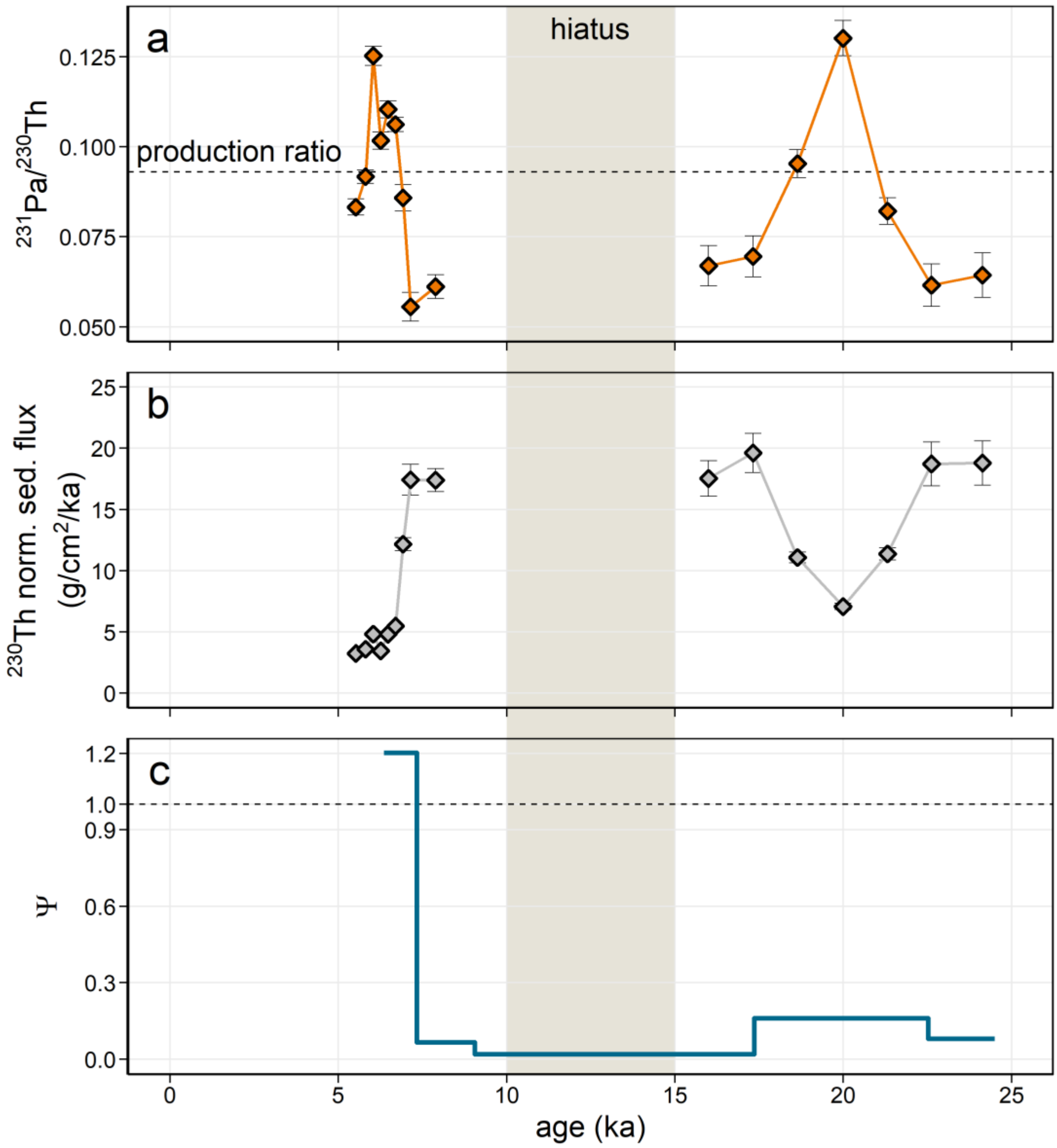

Fig. 5 The $^{231}Pa/^{230}Th$ (a) record of SU90-I02 compared to the ^{230}Th normalized sediment flux given in g/cm^2/ka (b) and the sediment focusing factor Ψ (c) calculated from $^{230}Th_{xs0}$ concentrations (Francois et al., 2004). High sediment fluxes correlated with the $^{231}Pa/^{230}Th$ activity ratios, indicative for a subordinate effect of the sediment flux on sedimentary $^{231}Pa/^{230}Th$. The dashed line in panel (a) indicates the production ratio of $^{231}Pa/^{230}Th$. The brown bar (hiatus) delineates the missing interval of the Deglacial in SU90-I02. The dashed line in panel (c) indicates a focusing factor of one which would indicate that now sediment is transported to or form this site. The strongest winnowing (sediment removal) is observed during the period of the proposed hiatus and is therefore in accordance with this finding.

4.4. The SU90-I02 $^{231}Pa/^{230}Th$ record interpreted in terms of reflecting AMOC variations

The here observed pattern of high Holocene and low Heinrich Stadial 1 and 2 $^{231}Pa/^{230}Th$ ratios is inverted and at first glance contradicting compared to the prominent $^{231}Pa/^{230}Th$ profiles from the deep northwestern Atlantic below 3000 m water depth (e.g. from the Bermuda Rise: McManus et al., 2004; Blake-Bahama Outer Ridge: Süfke et al., 2019; Ceara Rise: Lippold et al., 2016; Ng et al., 2018; Researchers Ridge: Ng et al., 2018) and time slice integrating compilations (Lippold et al., 2012a; Bradtmiller et al., 2014; Burckel et al., 2016).

However, the course of the SU90-I02 $^{231}Pa/^{230}Th$ matches the general glacial to Holocene evolution recorded by mid-depth North Atlantic site MD95-2037 at 2159 m (Gherardi et al., 2009; Fig. 1, 6). Both cores from shallower water depths share the same general pattern in their $^{231}Pa/^{230}Th$ profile with low values during prolonged cold periods (e.g. Heinrich Stadials) and a sharp increase to high Holocene values at ~ 8 ka. This pattern is inverted to the $^{231}Pa/^{230}Th$ profiles from the deep northwestern Atlantic (McManus et al., 2004; Lippold et al., 2009; Fig. 6) (low Holocene – high Glacial). Furthermore, the timing of the early Holocene circulation change is earlier (between 11 to 10 ka) in the deep compared the mid-depth Atlantic (see paragraph 4.5.; Fig. 6).

The position of a sediment core within one distinct overturning cell (in particular in terms of water depth) has been identified as a crucial parameter for $^{231}Pa/^{230}Th$, as suggested by simple box model approaches and observations (Luo et al., 2010; Lippold et al., 2011; Lippold et al., 2012a; Burckel et al., 2016). Further, the depth dependency of $^{231}Pa/^{230}Th$ is amplified with increasing circulation strength. A hypothetical static ocean would generate $^{231}Pa/^{230}Th$ deviations from the production ratio only due to large-scale diffusion caused by gradients in the particle fluxes between the margins and the inner ocean (boundary scavenging; Anderson et al., 1983; Hayes et al., 2015). But under a strong advection regime low $^{231}Pa/^{230}Th$ in deep waters predominantly result from the increasing vertically integrated deficit of ^{231}Pa relative to ^{230}Th. In shallower waters this deficit cannot build up efficiently due to the smaller water column above. Instead, dissolved ^{231}Pa is supplied from upstream while ^{230}Th is effectively scavenged to deeper waters leading to the observed decrease of $^{231}Pa/^{230}Th$ with water depth. However, shallower water depths alone seem not to be a sufficient condition for high $^{231}Pa/^{230}Th$. The Holocene $^{231}Pa/^{230}Th$ record at the Carolina Slope in a water depth of 1790 m (core KN140-2-51 GGC in the direct flow path of the Atlantic Deep Western Boundary Current; Hoffmann et al., 2018) displays constant values around 0.075 not exceeding the production ratio.

With adding this new mid-depth $^{231}Pa/^{230}Th$ record and reviewing the up-to-date available data base (McManus et al., 2004; Gherardi et al., 2009; Lippold et al., 2009,2011,2012a,2016; Bradtmiller et al., 2014; Böhm et al., 2015; Henry et al., 2016; Voigt et al., 2017; Mulitza et al., 2017; Ng et al., 2018;

Waelbroeck et al., 2018; Hoffmann et al., 2019; Süfke et al., 2019) on sedimentary $^{231}Pa/^{230}Th$ records from the western Atlantic, it becomes clear that even for a relatively constant mode of AMOC (as e.g. for the late Holocene) sedimentary $^{231}Pa/^{230}Th$ varies widely as a function of core location. As a consequence, predicting the behavior of $^{231}Pa/^{230}Th$ from a distinct position within a certain AMOC regime is unfortunately less intuitive. Accordingly, the use of adequate model approaches is necessary in order to better interpret $^{231}Pa/^{230}Th$ records (Luo et al., 2010; Rempfer et al., 2017).

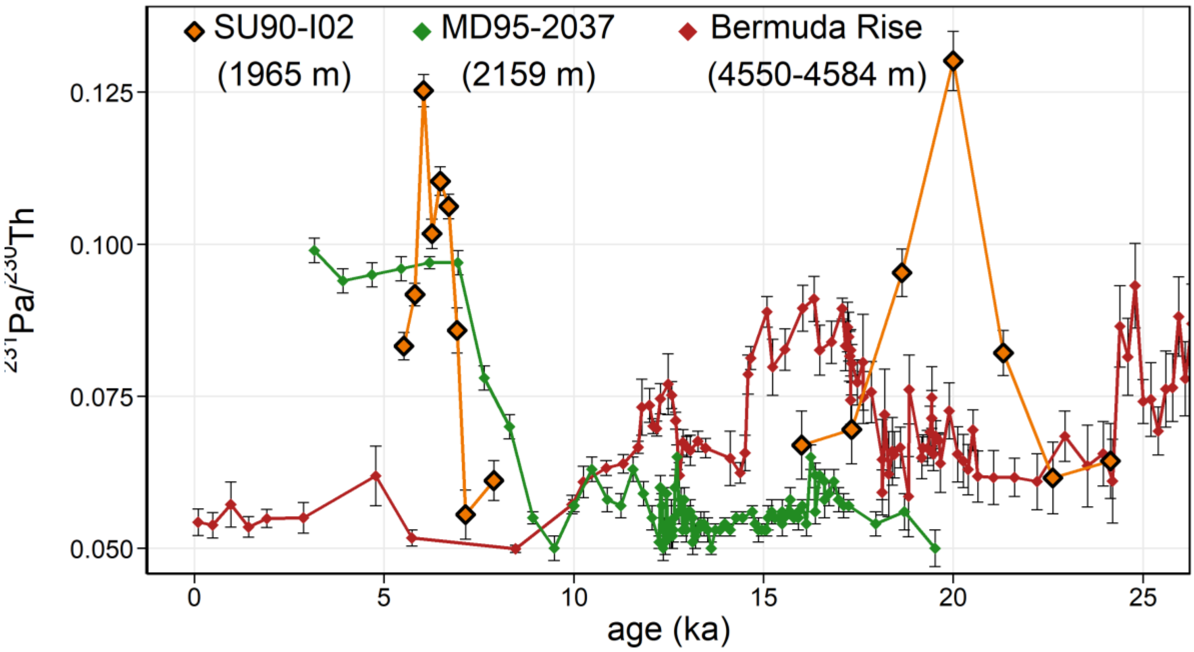

Fig. 6 $^{231}Pa/^{230}Th$ profiles of SU90-I02, MD95-2037 (Gherardi et al., 2009) and the Bermuda Rise (McManus et al., 2004; Lippold et al., 2009).

4.5. Modeled versus observed $^{231}Pa/^{230}Th$ at the mid-depth North Atlantic

There have been model approaches clearly pointing towards the importance of the core location on $^{231}Pa/^{230}Th$ (Siddall et al., 2007; Luo et al., 2010; Lippold et al., 2012; Rempfer et al., 2017; Van Hulten et al., 2018), but the observational $^{231}Pa/^{230}Th$ data hardly reaches the required coverage for unambiguous AMOC reconstructions.

With the Bern3D Earth System Model Rempfer et al. (2017) showed in transient experiments, in which the strength of the AMOC has been varied by changing freshwater forcing, a strong statistical anti-correlation between variations in AMOC strength and the particle-bound $^{231}Pa_p/^{230}Th_p$ in great depths in the Northwest Atlantic region (i.e. low AMOC produces high $^{231}Pa/^{230}Th$ and vice versa; Fig. 7). The authors improved the simulation of the protactinium and thorium cycle from older versions by taking additional sink processes into account (bottom scavenging; boundary scavenging; with/without particle redissolution at depth). They found the relationship between AMOC and $^{231}Pa/^{230}Th$ to be robust across these parametrizations, indicating that on larger spatial and temporal scales the relationship between $^{231}Pa/^{230}Th$ and AMOC is not fundamentally affected by uncertainties in the sink processes (e.g. bottom/boundary scavenging).

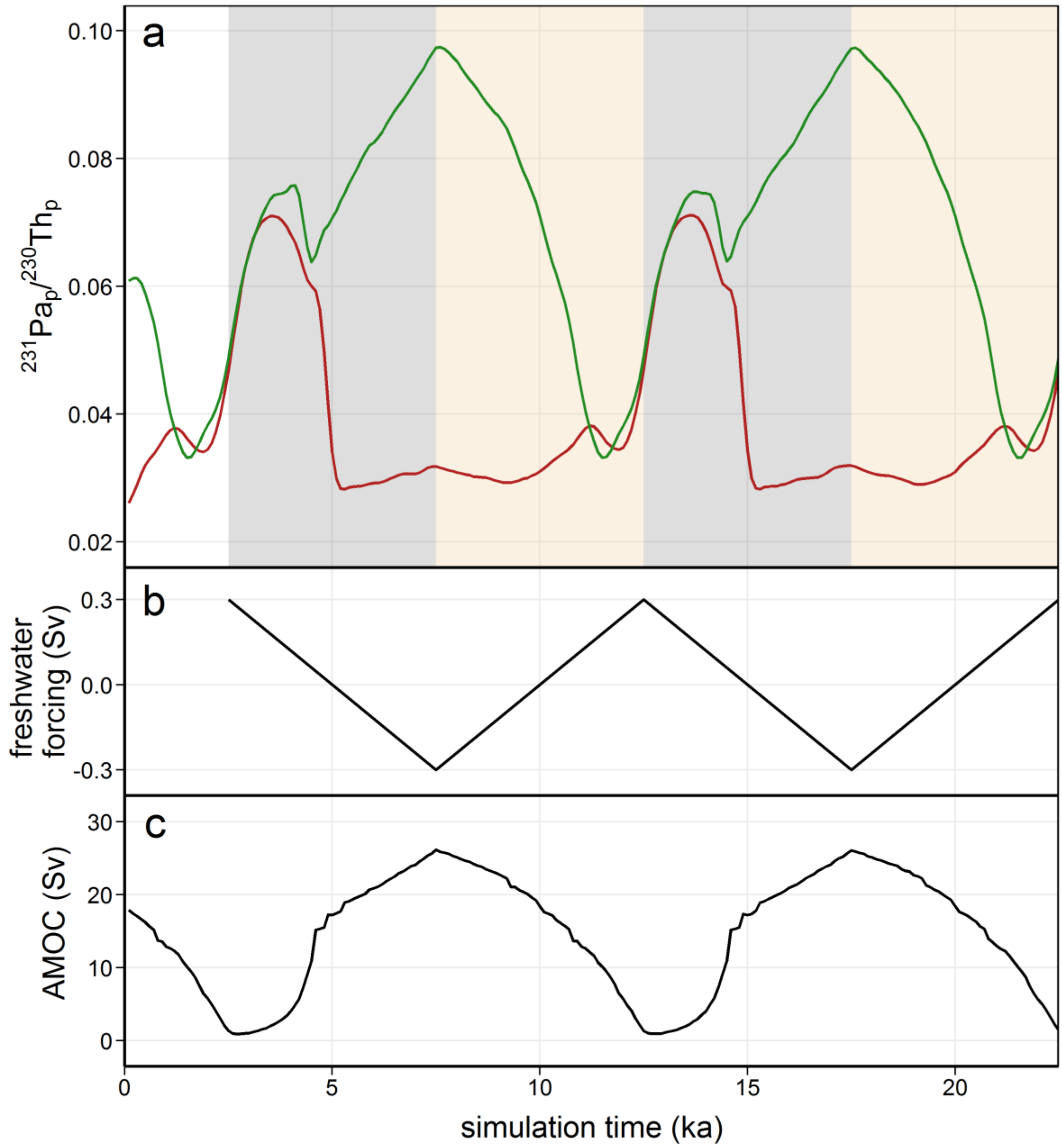

Fig. 7 (a) Bern3D model output of the $^{231}Pa/^{230}Th$ signal from simulation Re3d_Bd_Fw of Rempfer et al. (2017) for the grid cells closest to the core location of SU90-I02 (green) and for the deeper Bermuda Rise (red), which is also called Northwest Atlantic in Rempfer et al. (2017). (b) Amplitude of the North Atlantic freshwater forcing used by Rempfer et al. (2017), which causes the AMOC to fluctuate between 2 and 25 Sv. (c) The AMOC periodically fluctuates between practically no AMOC (2 Sv; e.g. at 2.5 ka) and a strong AMOC (25 Sv; e.g. at 7.5 ka) with a 10 kyr period. Gray bars indicate periods of increased AMOC strength (decreasing freshwater forcing), while light brown bars indicate decreasing AMOC (increasing freshwater forcing). The supplementary Fig. S4 indicates the used grid cells and shows the sign of $^{231}Pa/^{230}Th$ response to AMOC in different regions throughout the whole North Atlantic.

While the authors put emphasis on comparing the model outputs to the large observational data base available from the northwestern Atlantic (more specific the Bermuda Rise; McManus et al., 2004; Lippold et al., 2009; Henry et al., 2016), their model also reproduced observational features in other regions which have not yet received much attention. The figure 8a of Rempfer et al. (2017) shows a section plot of the North Atlantic (water depth versus latitude) indicating the correlation between AMOC strength and $^{231}Pa_p/^{230}Th_p$. For the northwestern Atlantic up to ~40°N and below ~2500 m water depth the negative model correlation corresponds to the classical picture as found in the Bermuda Rise sediment cores. Interestingly, for the region north of ~40°N and above ~2500 m water depth this correlation becomes inverted (strong AMOC causes higher $^{231}Pa/^{230}Th$). In this way, the modelling study of Rempfer et al. (2017) already predicted that sediment cores north of ~40°N should show a pattern of $^{231}Pa/^{230}Th$ vs. AMOC opposite to the expected, just as the results present in this study for core SU90-I02. For this study the model output of simulation Re3d_Bd_Fw of Rempfer et al. (2017) was revisited (see their Table A2 for parameters) without running new simulations. Thus, the AMOC fluctuations in our Figure 7c are equal to these presented in Rempfer et al. (2017) in their Figure 7a. The location of SU90-I02 indeed reveals a pattern highly sensitive on AMOC strength but asynchronous to the Bermuda Rise (Fig. 7). The main reason for this inverted behavior is grounded by the prevailing effect of import of ^{231}Pa over ^{230}Th from the upstream deep water formation zones as seen from the increase of $^{231}Pa_p$ with virtually unchanged $^{230}Th_p$ levels (Rempfer et al., 2017). Subsequently, further downstream and with increasing depth the ^{231}Pa deficit takes control due to meridional advection.

Furthermore, the model predicts a different response time of $^{231}Pa/^{230}Th$ variations in the deep (Bermuda Rise) and mid-depth Atlantic (e.g. SU90-I02) during increasing AMOC strength. After 2.5 ka of decreasing freshwater forcing (after 5 ka of simulation time in Fig. 7) $^{231}Pa/^{230}Th$ in the deep Atlantic reacts by a sharp decline from higher to lower values quickly reaching lowest levels which stays constant even during ongoing freshwater forcing. In contrast, after transient concordant behavior the mid-depth Atlantic shows a gradual increase in $^{231}Pa/^{230}Th$ after 2.5 ka of decreasing freshwater forcing with overall highest values at the lowest point of freshwater forcing and therefore strongest AMOC. This time lag between circulation change and $^{231}Pa/^{230}Th$ response at the mid-depth Atlantic compared to the deep Atlantic is reflected by the patterns seen in SU90-I02 and MD95-2037. Both cores show low $^{231}Pa/^{230}Th$ values during the early Holocene while the deep Atlantic already shows low $^{231}Pa/^{230}Th$ values (Fig. 6) indicating a strong circulation (the mid-depth cores are supposed to show high values during a strong AMOC, Fig. S5). The time lag between decreasing $^{231}Pa/^{230}Th$ values in the deep Atlantic and increasing values in the mid-depth Atlantic is in the order of 2-4 ka (Fig. 6) which is similar to the model findings (Fig. 7). Therefore, the model findings do not only predicts the general direction of $^{231}Pa/^{230}Th$ change under variations in AMOC strength at a given position in the West Atlantic Overturning cell but also the relative timing.

Conclusions

Sedimentary analyses of the mid-depth North Atlantic core SU90-I02 result in a classical picture of IRD dominated sediments for Heinrich Stadials 1 and 2. Changes in sedimentology corresponding to the climatic periods of Heinrich Stadial 1 and 2, the LGM and the Holocene are clearly resolvable. The new established $^{231}Pa/^{230}Th$ down core profile from SU90-I02 reveals $^{231}Pa/^{230}Th$ values higher than the production ratio during periods of strong AMOC, such as the Holocene. The effect of the particle flux and enhanced scavenging of protactinium is found minor during these periods. Hence, the sedimentary $^{231}Pa/^{230}Th$ of this core at 45°N shows an opposite behavior compared to deep Atlantic sites (e.g. the Bermuda Rise) with values clearly below the production ratio during cold phases, like Heinrich Stadials 1 and 2. However, findings from the Bern3D model (e.g. Rempfer et al., 2017) confirm such an oppositional behavior in $^{231}Pa/^{230}Th$ between the deep northwestern and the mid-depth northern Atlantic north of 40°N. This model predicts that $^{231}Pa/^{230}Th$ from mid-depth sites north of 40°N correlate positively with the AMOC strength. This study adds a further downcore profile to the still sparse Atlantic $^{231}Pa/^{230}Th$ data-base and highlights the importance of considering the core position for interpretations of $^{231}Pa/^{230}Th$ ratios, even inside the same overturning cell. By combining spatially distributed, well dated and synchronized $^{231}Pa/^{230}Th$ records in the Atlantic Ocean much tighter constraints can be placed on changes in deep ocean circulation pathways and water mass distributions.

Acknowledgment

We thank Isabelle Billy from the University of Bordeaux and Claire Waelbroeck and Elisabeth Michel from the LSCE in Paris for providing the samples of SU90-I02 for the $^{231}Pa/^{230}Th$ and XRF analysis. XRF measurements were supported by Andreas Koutsodendris and Siphon de Finès was always supportive during laboratory work. We acknowledge the constructive comments of two anonymous reviewers. This study has been funded by the Emmy-Noether-Programm of the German Research Foundation (DFG) Grant Li1815/4.

References

Anderson RF, Bacon MP, Brewer PG (1983) Removal of 230Th and 231Pa at ocean margins. Earth Planet Sci Lett 66:73–90. doi: 10.1016/0012-821X(83)90127-9

Andrews JT, Tedesco K (1992) Detrital carbonate-rich sediments, northwestern Labrador Sea: implications for ice-sheet dynamics and iceberg rafting (Heinrich) events in the North Atlantic. Geology 20:1087–1090. doi: 10.1130/0091-7613(1992)020<1087:DCRSNL>2.3.CO;2

Andrews JT, Voelker AHL (2018) “Heinrich events” (& sediments): A history of terminology and recommendations for future usage. Quat Sci Rev 187:31–40. doi: 10.1016/j.quascirev.2018.03.017

Bandy OL (1972) Origin and Development of Globorotalia (Turborotalia) pachyderma (Ehrenberg). Micropaleontology 18:294. doi: 10.2307/1485010

Banner FT, Blow WH (1960) Some primary types of species belonging to the superfamily Globigerinaceae. Contrib from Cushman Found Foraminifer Res 11:1–41

Böhm E, Lippold J, Gutjahr M, et al (2015) Strong and deep Atlantic meridional overturning circulation during the last glacial cycle. Nature 517:73–76. doi: 10.1038/nature14059

Bond G, Heinricht H, Broecker W, et al (1992) Evidence for massive discharges of icebergs into the North Atlantic ocean during the last glacial period. Nature 360:245-249. doi: 10.1038/360245a0

Bradtmiller LI, McManus JF, Robinson LF (2014) 231Pa/230Th evidence for a weakened but persistent Atlantic meridional overturning circulation during Heinrich Stadial 1. Nat Commun 5:5817. doi: 10.1038/ncomms6817

Broecker W, Bond G, Klas M, Clark E, McManus J (1992) Origin of the northern Atlantic's Heinrich events. Climate Dynamics 6:265–273. doi: 10.1007/BF00193540

Broecker WS, Bond G, Klas M (1990) A salt oscillator in the glacial Atlantic. Paleoceanography 5:469–477. doi: 10.1029/PA005i004p00469

Burckel P, Waelbroeck C, Luo Y, et al (2016) Changes in the geometry and strength of the Atlantic meridional overturning circulation during the last glacial (20-50 ka). Clim Past 12:2061–2075. doi: 10.5194/cp-12-2061-2016

Chase Z, Anderson RF, Fleisher MQ, Kubik PW (2002) The influence of particle composition and particle flux on scavenging of Th, Pa and Be in the ocean. Earth Planet Sci Lett 204:215–229. doi: 10.1016/S0012-821X(02)00984-6

Chase Z, Anderson RF, Fleisher MQ, Kubik PW (2003) Scavenging of 230Th, 231Pa and 10Be in the Southern Ocean (SW Pacific sector): The importance of particle flux, particle composition and advection. Deep Res Part II Top Stud Oceanogr 50:739–768. doi: 10.1016/S0967-0645(02)00593-3

Chase Z, Anderson RF (2004) Comment on "On the importance of opal, carbonate, and lithogenic clays in scavenging and fractionating 230 Th, 231 Pa and 10 Be in the ocean" by S. Luo and T.-L. Ku. Earth Planet Sci Lett 220:213–222. doi: 10.1016/S0012-821X(04)00028-7

Christl M, Lippold J, Hofmann A, et al (2010) 231Pa/230Th: A proxy for upwelling off the coast of West Africa. Nucl Instruments Methods Phys Res Sect B Beam Interact with Mater Atoms 268:1159–1162. doi: 10.1016/j.nimb.2009.10.123

Clark PU, Marshall SJ, Clarke GKS, et al (2001) Freshwater Forcing of Abrupt Climate Change During the Last Glaciation. Science 293:283–287. doi: 10.1126/science.1062517

Duplessy JC, Labeyrie L, Arnold M, et al (1992) Changes in surface salinity of the North Atlantic Ocean during the last deglaciation. Nature 358:485–488. doi: 10.1038/358485a0

Ferreira ML de C, Kerr R (2017) Source water distribution and quantification of North Atlantic Deep Water and Antarctic Bottom Water in the Atlantic Ocean. Prog Oceanogr 153:66–83. doi: 10.1016/j.pocean.2017.04.003

Fietzke J, Bollhöfer A, Frank M, Mangini A (1999) Protactinium determination in manganese crust VA13/2 by thermal ionization mass spectrometry (TIMS). Nucl Instruments Methods Phys Res Sect B Beam Interact with Mater Atoms 149:353–360. doi: 10.1016/S0168-583X(98)00912-4

Francois R, Frank M, Rutgers van der Loeff MM, Bacon MP (2004) 230 Th normalization: An essential tool for interpreting sedimentary fluxes during the late Quaternary. Paleoceanography 19. doi: 10.1029/2003PA000939

Geibert W, Usbeck R (2004) Adsorption of thorium and protactinium onto different particle types: Experimental findings. Geochim Cosmochim Acta 68:1489–1501. doi: 10.1016/j.gca.2003.10.011

Gherardi JM, Labeyrie L, McManus JF, et al (2005) Evidence from the Northeastern Atlantic basin for variability in the rate of the meridional overturning circulation through the last deglaciation. Earth Planet Sci Lett 240:710–723. doi: 10.1016/j.epsl.2005.09.061

Gherardi JM, Labeyrie L, Nave S, et al (2009) Glacial-interglacial circulation changes inferred from231Pa/ 230Th sedimentary record in the North Atlantic region. Paleoceanography 24:1–14. doi: 10.1029/2008PA001696

Gottschalk J, Szidat S, Michel E, et al (2018) Radiocarbon measurements of small-size foraminiferal samples with the MIni CArbon DAting System (MICADAS) at the University of Bern: implications for paleoclimate reconstructions. Radiocarbon 60:469-491. doi: 10.1017/RDC.2018.3

Grousset FE, Cortijo E, Huon S, et al (2001) Zooming in on Heinrich layers. Paleoceanography 16:240–259. doi: 10.1029/2000PA000559

Gu S, Liu Z (2017) 231Pa and 230Th in the ocean model of the Community Earth System Model (CESM1.3). Geosci Model Dev 10:4723–4742. doi: 10.5194/gmd-10-4723-2017

Hall IR, Moran SB, Zahn R, et al (2006) Accelerated drawdown of meridional overturning in the late-glacial Atlantic triggered by transient pre-H event freshwater perturbation. Geophys Res Lett 33:1–5. doi: 10.1029/2006GL026239

Hayes CT, Anderson RF, Fleisher MQ, et al (2015a) 230Th and 231Pa on GEOTRACES GA03, the U.S. GEOTRACES North Atlantic transect, and implications for modern and paleoceanographic chemical fluxes. Deep Res Part II Top Stud Oceanogr 116:29–41. doi: 10.1016/j.dsr2.2014.07.007

Hayes CT, Anderson RF, Fleisher MQ, et al (2015b) Intensity of Th and Pa scavenging partitioned by particle chemistry in the North Atlantic Ocean. Mar Chem 170:49–60. doi: 10.1016/j.marchem.2015.01.006

Heinricht H (1988) Origin and Consequences of Cyclic Ice Rafting in the Northeast Atlantic Ocean during the Past 130,000 Years. Quat Res 29:142–152. doi: 10.1016/0033-5894(88)90057-9

Hemming SR (2004) Heinrich events: Massive late Pleistocene detritus layers of the North Atlantic and their global climate imprint. Rev Geophys 42:1-43. doi: 10.1029/2003RG000128

Henderson GM, Anderson RF (2003) The U-series Toolbox for Paleoceanography. Rev Mineral geochemistry 52:493–531. doi: 10.2113/0520493

Henry LG, McManus JF, Curry WB, et al (2016) North Atlantic ocean circulation and abrupt climate change during the last glaciation. Science 353:470–474. doi: 10.1126/science.aaf5529

Hodell DA, Channeil JET, Curtis JH, et al (2008) Onset of “Hudson Strait” Heinrich events in the eastern North Atlantic at the end of the middle Pleistocene transition (∼640 ka)? Paleoceanography 23:1–16. doi: 10.1029/2008PA001591

Hodell DA, Nicholl JA, Bontognali TRR, et al (2017) Anatomy of Heinrich Layer 1 and its role in the last deglaciation. Paleoceanography 32:284–303. doi: 10.1002/2016PA003028

Hoffmann SS, McManus JF, Swank E. (2018) Evidence for Stable Holocene Basin-Scale Overturning Circulation Despite Variable Currents Along the Deep Western Boundary of the North Atlantic Ocean. Geophys Res Lett 45:1–10. doi: 10.1029/2018GL080187

Jullien E, Grousset FE, Hemming SR, et al (2006) Contrasting conditions preceding MIS3 and MIS2 Heinrich events. Glob Planet Change 54:225–238. doi: 10.1016/j.gloplacha.2006.06.021

Kretschmer S, Geibert W, Rutgers van der Loeff MM, et al (2011) Fractionation of 230Th, 231Pa, and 10Be induced by particle size and composition within an opal-rich sediment of the Atlantic Southern Ocean. Geochim Cosmochim Acta 75:6971–6987. doi: 10.1016/j.gca.2011.09.012

Kretschmer S, Geibert W, Rutgers van der Loeff MM, Mollenhauer G (2010) Grain size effects on 230 Thxs inventories in opal-rich and carbonate-rich marine sediments. Earth Planet Sci Lett 294:131–142. doi: 10.1016/j.epsl.2010.03.021Kucera M (2007) Chapter Six Planktonic Foraminifera as Tracers of Past Oceanic Environments. Dev Mar Geol 1:213–262. doi: 10.1016/S1572-5480(07)01011-1

Labeyrie AL, Vidal L, Cortijo E, et al (1995) Surface and deep hydrology of the Northern Atlantic Ocean during the past 150000 years. Philos Trans R Soc London Ser B Biol Sci 348:255–264. doi: 10.1098/rstb.1995.0067

Lambelet M, van de Flierdt T, Crocket K, et al (2016) Neodymium isotopic composition and concentration in the western North Atlantic Ocean: Results from the GEOTRACES GA02 section. Geochim Cosmochim Acta 177:1–29. doi: 10.1016/j.gca.2015.12.019

Lippold J, Grützner J, Winter D, et al (2009) Does sedimentary 231Pa/230Th from the Bermuda Rise monitor past Atlantic Meridional Overturning Circulation? Geophys Res Lett 36:1–6. doi: 10.1029/2009GL038068

Lippold J, Gherardi JM, Luo Y (2011) Testing the 231Pa/230Th paleocirculation proxy: A data versus 2D model comparison. Geophys Res Lett 38:1–7. doi: 10.1029/2011GL049282

Lippold J, Luo Y, Francois R, et al (2012a) Strength and geometry of the glacial Atlantic Meridional Overturning Circulation. Nat Geosci 5:813–816. doi: 10.1038/ngeo1608

Lippold J, Mulitza S, Mollenhauer G, et al (2012b) Boundary scavenging at the East Atlantic margin does not negate use of 231Pa/ 230Th to trace Atlantic overturning. Earth Planet Sci Lett 333–334:317–331. doi: 10.1016/j.epsl.2012.04.005

Lippold J, Gutjahr M, Blaser P, et al (2016) Deep water provenance and dynamics of the (de)glacial Atlantic meridional overturning circulation. Earth Planet Sci Lett 445:68–78. doi: 10.1016/j.epsl.2016.04.013

Luo Y, Francois R, Allen S (2010) Sediment 231Pa/230Th as a recorder of the rate of the Atlantic meridional overturning circulation: insights from a 2-D model. Ocean Sci 6:381–400. doi: 10.5194/os-6-381-2010

Lynch-Stieglitz J (2017) The Atlantic Meridional Overturning Circulation and Abrupt Climate Change. Ann Rev Mar Sci 9:83–104. doi: 10.1146/annurev-marine-010816-060415

Manighetti B, McCave IN, Maslin M, Shackleton NJ (1995) Chronology for climate change: Developing age models for the biogeochemical ocean flux study cores. Paleoceanography 10:513–525. doi: 10.1029/94PA03062

Marchal O, Francois R, Stocker TF, Joos F (2000) Ocean thermohaline circulation and sedimentary 231Pa/230Th ratio. Paleoceanography 15:625–641. doi: 10.1029/2000PA000496

McManus JF, Francois R, Gherardi J-M, et al (2004) Collapse and rapid resumption of Atlantic meridional circulation linked to deglacial climate changes. Nature 428:834–837. doi: 10.1038/nature02494

Missiaen L, Pichat S, Waelbroeck C, et al (2018) Downcore Variations of Sedimentary Detrital (238U/232Th) Ratio: Implications on the Use of230Thxsand231Paxsto Reconstruct Sediment Flux and Ocean Circulation. Geochemistry, Geophys Geosystems 19:2560–2573. doi: 10.1029/2017GC007410

Mulitza S, Chiessi CM, Schefuß E, et al (2017) Synchronous and proportional deglacial changes in Atlantic meridional overturning and northeast Brazilian precipitation. Paleoceanography 32:622–633. doi: 10.1002/2017PA003084

Müller PJ, Schneider R (1993) An automated leaching method for the determination of opal in sediments and particulate matter. Deep Res Part I 40:425–444. doi: 10.1016/0967-0637(93)90140-X

Ng HC, Robinson LF, McManus JF, et al (2018) Coherent deglacial changes in western Atlantic Ocean circulation. Nat Commun 9:1–10. doi: 10.1038/s41467-018-05312-3

Pham MK, Sanchez-Cabeza JA, Povinec PP, et al (2008) A new Certified Reference Material for radionuclides in Irish sea sediment (IAEA-385). Appl Radiat Isot 66:1711–1717. doi: 10.1016/j.apradiso.2007.10.020

Rashid H, Boyle EA (2007) Mixed-Layer Deepening During Heinrich Events : A Multi-Planktonic Foraminiferal δ18O Approach. Science 318:439–441. doi: 10.1126/science.1146138

Reimer PJ, Bard E, Bayliss A, et al. (2013) IntCal13 and Marine13 radiocarbon age calibration curves 0-50,000 years cal BP. Radiocarbon 55:1869-1887. doi: 10.2458/azu_js_rc.55.16947

Regelous M, Turner SP, Elliott TR, et al (2004) Measurement of femtogram quantities of protactinium in silicate rock samples by multicollector inductively coupled plasma mass spectrometry. Anal Chem 76:3584–3589. doi: 10.1021/ac030374l

Rempfer J, Stocker TF, Joos F, et al (2017) New insights into cycling of 231 Pa and 230 Th in the Atlantic Ocean. Earth Planet Sci Lett 468:27–37. doi: 10.1016/j.epsl.2017.03.027

Roberts NL, McManus JF, Piotrowski AM, McCave IN (2014) Advection and scavenging controls of Pa/Th in the northern NE Atlantic. Paleoceanography 29:668–679. doi: 10.1002/2014PA002633

Roche D, Paillard D, Cortijo E (2004) Constraints on the duration and freshwater release of Heinrich event 4 through isotope modelling. Nature 432:379–382. doi: 10.1038/nature03059

Ruddiman WF (1977) North atlantic ice-rafting: A major change at 75,000 years before the present. Science 196:1208–1211. doi: 10.1126/science.196.4295.1208

Rutgers van der Loeff M, Venchiarutti C, Stimac I, et al (2016) Meridional circulation across the Antarctic Circumpolar Current serves as a double 231Pa and 230Th trap. Earth Planet Sci Lett 455:73–84. doi: 10.1016/j.epsl.2016.07.027

Schiebel R and Hemleben C (2017). Planktic Foraminifera in the Modern Ocean. Springer, Berlin Heidelberg 333pp. ISBN 978-3-662-50297-6

Schulz H (1995a) Planktic foraminifera assemblage in sediment core SU90-I02. Pangaea. doi: 10.1594/PANGAEA.134148

Schulz H (1995b) Stable isotope analysis on planktic foraminifera in sediment core SU90-I02. Pangaea. doi: 10.1594/PANGAEA.107750

Siddall M, Stocker TF, Henderson GM, et al (2007) Modeling the relationship between 231Pa/230Th distribution in North Atlantic sediment and Atlantic meridional overturning circulation. Paleoceanography 22:1–14. doi: 10.1029/2006PA001358

Storz D, Schulz H, Waniek JJ, et al (2009) Seasonal and interannual variability of the planktic foraminiferal flux in the vicinity of the Azores Current. Deep Res Part I Oceanogr Res Pap 56:107–124. doi: 10.1016/j.dsr.2008.08.009

Süfke F, Lippold J, Happel S (2018) Improved Separation of Pa from Th and U in Marine Sediments with TK400 Resin. Anal Chem 90:1395–1401. doi: 10.1021/acs.analchem.7b04723

Süfke F, Pöppelmeier F, Goepfert TJ, et al (2019) Constraints on the northwestern Atlantic deep water circulation from 231Pa/230Th during the last 30,000 years. Paleoceanography and Paleoclimatology (accepted). doi: 10.1029/2019PA003737

Szidat S, Salazar GA, Vogel E, et al (2014) ^{14}C analysis and sample preparation at the new Bern Laboratory for the Analysis of Radiocarbon with AMS (LARA). Radiocarbon 56:561–566. doi: 10.2458/56.17457

Waelbroeck C, Pichat S, Böhm E, et al (2018) Relative timing of precipitation and ocean circulation changes in the western equatorial Atlantic over the last 45 kyr. Clim Past 14:1315–1330. doi: 10.5194/cp-14-1315-2018

Watkins SJ, Maher BA, Bigg GR (2007) Ocean circulation at the Last Glacial Maximum: A combined modeling and magnetic proxy-based study. Paleoceanography 22:1–20. doi: 10.1029/2006PA001281

Van Hulten M, Dutay JC, Roy-Barman M (2018) A global scavenging and circulation ocean model of thorium-230 and protactinium-231 with improved particle dynamics (NEMO-ProThorP 0.1). Geosci Model Dev 11:3537–3556. doi: 10.5194/gmd-11-3537-2018

Voigt I, Cruz APS, Mulitza S, et al (2017) Variability in mid-depth ventilation of the western Atlantic Ocean during the last deglaciation. Paleoceanography 1–18. doi: 10.1002/2017PA003095

Yu E-F, Francois R, Bacon MP (1996) Similar rates of modern and last-glacial ocean thermohaline circulation inferred from radiochemical data. Nature 379:689–694. doi: 10.1038/379689a0